Torque Envelope Control for Four-Wheel-Drive Electric Vehicles

Chuantang Xiong * **Yang Xu** ** **Fan Yu** *** **Chengbin Ma** ****

* *University of Michigan-Shanghai Jiao Tong University Joint Institute, Shanghai 200240, China (e-mail: Davidxiong@sjtu.edu.cn).*
** *University of Michigan-Shanghai Jiao Tong University Joint Institute, Shanghai 200240, China (e-mail: xuyang163@sjtu.edu.cn)*
*** *School of Mechanical Engineering, Shanghai Jiao Tong University, Shanghai 200240, China (e-mail: fanyu@sjtu.edu.cn')*
**** *University of Michigan-Shanghai Jiao Tong University Joint Institute, Shanghai 200240, China (e-mail: chbma@sjtu.edu.cn)*

Abstract: This paper proposes a novel torque envelope control specified for electric vehicles. The basic idea is to restrict the drive motor torque and thus limit the over-acceleration in vehicle longitudinal direction. This in turn preserves the capability for the necessary lateral acceleration that maintains the vehicle stability. In this paper, first the road/tire interactions in both longitudinal and lateral directions are reviewed; then the approximate homogeneity and simultaneity of the road/tire interactions are explained; based on those preliminary discussions, the envelope control of the electric drive motor torque is developed accordingly; finally, the proposed control is validated through simulation under various driving conditions.

Keywords: electric vehicle, envelope control, vehicle stability, accelerometer.

1. INTRODUCTION

Electric Vehicles (EVs) are widely considered as one of solutions for mitigating global warming and protection of environment. Compared with traditional vehicles, EVs are obviously more energy-efficient and thus "greener". But actually at the same time, thanks to the quick and accurate response of electric drive motors, the safety of driving can also be significantly improved through advance electric vehicle dynamics.

Currently, Electronic Stability Program(ESP) is widely implemented in today's conventional road vehicles as a vehicle stability control function [Van Zanten (2000)][Liebemann et al. (2004)]. The action of the ESP is usually based on ON-OFF control of brakes. Since the torque (both for braking and driving) of the electric drive motors can be accurately controlled, theoretically electric vehicles could achieve a higher-level stability control performance. This aspect of electric vehicles has been discussed in literature. In [Hori et al. (1998)] a model-following-based traction control is developed for electric vehicles. Other approaches for the EV longitudinal dynamics were proposed later such as through fuzzy control and neural networks, and the acceleration-to-torque ratio based anti-skid control [Tahami et al. (2003)][Wu et al. (2015)]. Meanwhile, it is more challenging to maintain stability during cornering, i.e., the lateral dynamics, because the lateral motion and traction force are difficult to directly measure and control. There are various solutions including direct yaw moment control and lateral stability control [Nam et al. (2012)][Chen and Wang (2013)]. However, the drawback of these methods is that they need expensive sensors such as high-accuracy GPS and lateral tire force sensor for the feedback-based control. The complicated calculations are also required to estimate the parameters such as the desired yaw angle β and the yaw rate γ. And the time-consuming calculations need to be continuously run even the vehicle is being driving normally. Thus this may also unnecessarily interfere the normal driving of the vehicle.

In order to overcome the above disadvantages, this paper develops a novel torque envelop control that ensures both the longitudinal and lateral stability. It only requires a small amount of calculation based on the feedback signals from a standard on-board accelerometer and encoders of the electric drive motors. Besides, the envelope control does not interfere normal vehicle driving. This paper is organized as follows: in section 2 the road/tire interactions in both longitudinal and lateral directions are reviewed in detail; the approximate homogeneity and simultaneity of the road/tire interactions are then explained; based on those preliminary discussions, in section 3 the envelope control of the electric drive motor torque is developed accordingly; finally, in section 4 the proposed control is validated through simulation under various driving conditions.

2. REVIEW OF TIRE/ROAD INTERACTIONS

Here the analysis of both the longitudinal and lateral interactions between tire and road is based on the well-known Magic Formula [Pacejka and Bakker (1992)]. This model is widely used when discussing vehicle dynamics.

[1] This work is supported by National Science Foundation of China [grant number 51305259 and 51375299].

2.1 Approximate homogeneity

Essentially the interaction between tire and road is due to the deformation of the rubber. The characteristic of the rubber plays a vital role in the tire/road interactions. Although there are some differences such as in geometric structure and deformation stiffness in the longitudinal and lateral directions, basically forces at the two directions share similar nature and changing trend. It is known that both the longitudinal and lateral traction/friction forces can be represented by the Magic Formula in a same form:

$$y = D\sin\left\{C\tan^{-1}\left[Bx - E\left(Bx - \tan^{-1}Bx\right)\right]\right\}. \quad (1)$$

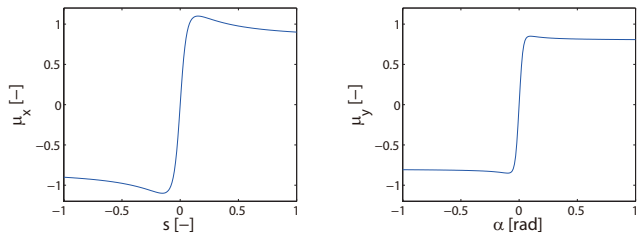

(a) Longitudinal direction (b) Lateral direction

Fig. 1. Relationships between friction coefficients and slip coefficients.

As shown in Fig. 1, s and α are the slip ratio and slip angle; μ_x and μ_y are the friction coefficients in longitudinal and lateral direction, respectively. In order to maintain the stability of the vehicle, tires are required to operate in the linear region, i.e., the region where both α and s are usually less than 0.1. Only within this region the torque applied on wheel (i.e., the desired acceleration of the driver), the vehicle velocity, and the traction force are almost linearly dependent and controllable.

In order to explore the two-dimensional relationship between slip coefficients and friction coefficients, the four parameters are combined into two vectors, i.e., the slip coefficient vector $\overrightarrow{S} = (s, \alpha)$ and the friction coefficient vector $\overrightarrow{M} = (\mu_x, \mu_y)$, and $\overrightarrow{M}$ is projected on $\overrightarrow{S}$ plane as shown in Fig. 2.

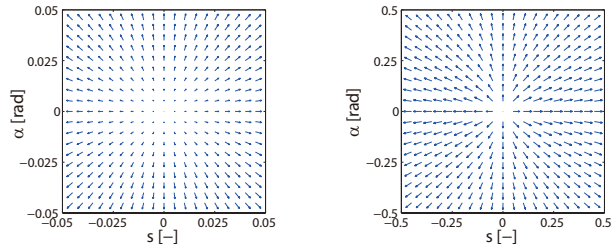

(a) Slip coefficients ranging from -0.05 to 0.05 (b) Slip coefficients ranging from -0.5 to 0.5

Fig. 2. Projection of friction coefficients on slip coefficient plane

In Fig. 2 the blue arrows represent the vector $\overrightarrow{M}$. Here two preliminary observations can be made:

(1) The direction of $\overrightarrow{S}$ is nearly as same as that of $\overrightarrow{M}$. The difference is only within 5° at most. Therefore, $\overrightarrow{S}$ and $\overrightarrow{M}$ can be approximately considered as the vectors with a same direction, and only their relationship in modules needs to be discussed, namely $|\overrightarrow{M}| = f(|\overrightarrow{S}|)$.

(2) When $|\overrightarrow{S}|$ is small, $|\overrightarrow{M}|$ grows with $|\overrightarrow{S}|$; while if $|\overrightarrow{S}|$ becomes too large, $|\overrightarrow{M}|$ does not change much.

For reference purposes, the two and three-dimensional relationships among the module of $|\overrightarrow{M}|$, s, and α are also shown in Fig. 3.

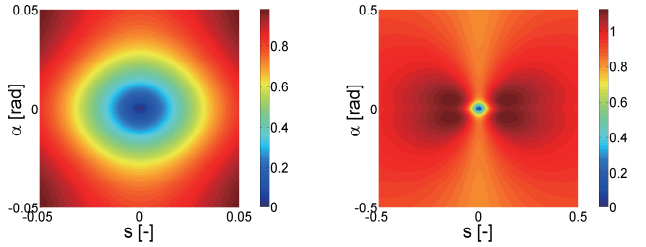

(a) Slip coefficients ranging from -0.05 to 0.05 (b) Slip coefficients ranging from -0.5 to 0.5

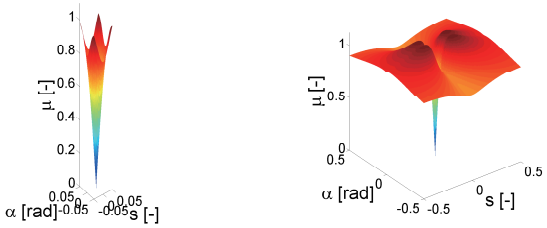

(c) Slip coefficients ranging from -0.05 to 0.05 (d) Slip coefficients ranging from -0.5 to 0.5

Fig. 3. The two and three-dimensional relationships.

Based on Figs. 2 and 3, the below conclusions can be drawn that serve as a basis for the following discussion:

(1) When $|\overrightarrow{S}|$ is small, $\overrightarrow{M}$ grows almost linearly with $\overrightarrow{S}$ in both longitudinal and lateral directions, and the two vectors do not interfere with each other;

(2) When $|\overrightarrow{S}|$ is too large, $|\overrightarrow{M}|$ reaches its upper limit and only the direction of $\overrightarrow{M}$ changes. Thus the increase of traction force in one direction will sacrifice the traction force or capability in another direction.

2.2 Approximate simultaneity

In an ideal case where there is no limit of $|\overrightarrow{M}|$, any torque applied on the wheel will generate desired $\overrightarrow{M}$ and $\overrightarrow{S}$, and the tires always operate in their stable regions. However, in reality due to the limit of the traction force when driving on a specific road surface, once the applied torque commanded by the driver is too large, the tire can no longer provide sufficient traction force. This leads to a rapid increase of $|\overrightarrow{S}|$ and makes the vehicle become uncontrollable. In this extreme situation where $|\overrightarrow{M}|$ reaches its upper limit (i.e., the envelope), but the direction of $\overrightarrow{M}$ is still almost as same as $\overrightarrow{S}$.

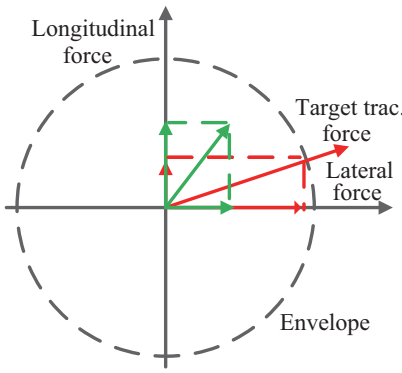

Fig. 4. Examples of controllable state (green arrow) and uncontrollable state (red arrow) in both directions.

As illustrated in Fig. 4, even the longitudinal slip is very small($s \ll 0.1$), but if the lateral slip is too large ($\alpha \gg 0.2$), the traction force in longitudinal direction may still go beyond its current limit or envelope, and vice versa. Therefore,

(1) When the applied wheel torque is small, s lies in its linear region, and sufficient traction forces can be provided simultaneously in both directions. Thus the motion of the vehicle is stable and controllable;
(2) When the applied torque is excessively large, s lies in its nonlinear region, and the traction force in the longitudinal direction reaches its upper limit. Thus tire can not generate required traction forces in not only longitudinal but also lateral directions. This makes the motion of the vehicle simultaneously uncontrollable in both directions.

As a conclusion, the stability in the longitudinal and lateral directions relate to each other and will be violated at the same time. Therefore, the measurement of the lateral motion of the vehicles such as lateral velocity, lateral force, and yaw angle can be avoided by making full of the longitudinal dynamics control. Especially for electric vehicles, the longitudinal slip can be directly measured because the torque applied to the wheel can be accurately obtained from the current feedback of the electric drive motors. Thanks to the advantage of the electric drive and the homogeneity and simultaneity of tire/road interactions in the longitudinal and lateral directions, the lateral stability of electric vehicles can be indirectly estimated from their longitudinal motion.

3. CONTROL STRATEGY

In this section the strategy of the torque envelope control is discussed. This strategy requires feedback of the target centripetal vehicle acceleration from the driver. Then the control flow is explained using equations and a flow chart. In the control strategy the electric motor torque command from the driver is limited by a derived envelope in order to maintain the vehicle stability.

3.1 Basic consideration

It is well-known that the lateral vehicle dynamics is difficult to be directly regulated; while usually the longitudinal dynamics is relatively easy to be measured and controlled. Thus the essence of the control strategy here is to first satisfy the requirement of lateral acceleration; if there is still capacity within the limit of the total acceleration (i.e., the envelope), this capacity can be assigned to meet the requirement of longitudinal acceleration. Fig. 5 illustrates several different cases, where a_n and a_t are the normal/centripetal and tangential accelerations of the vehicle motion, respectively. In the figure the green broken line and solid line represent the required and real normal acceleration (≈lateral acceleration), respectively; while the red broken line is the limit of the maximum permissible tangential acceleration, which is also close to the longitudinal acceleration.

It should be noticed that in a normal driving condition the vehicle lateral motion is usually not significant even during cornering. In general the steering angle is also small, and thus the tangential trajectory can be approximately considered as same as the longitudinal trajectory. Thus a_n approximately equals a_y that determines the lateral vehicle stability. This characteristic makes it possible to approximately represent the required lateral acceleration by the target normal or centripetal acceleration of the driver.

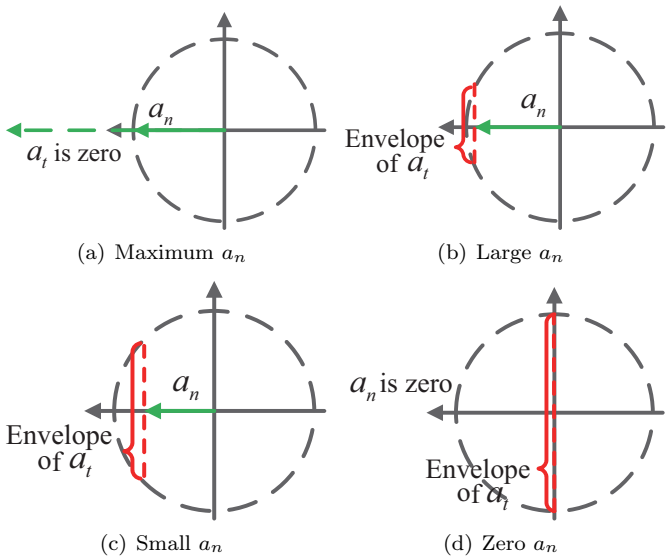

Fig. 5. Envelope of normal and tangential accelerations.

3.2 Target centripetal acceleration

The target centripetal acceleration can be determined assuming small slip ratio. Then the vehicle velocity is close to the wheel velocity, and the curvature of motion trajectory is approximately as equal as the steering angle. The advantage of the assumptions is that all required parameters are now measurable. According to the Ackermann steering principle, the relationships can be expressed as [Siegwart et al. (2011)]:

$$\begin{cases} v_x \approx \omega_w r_w \\ R \approx \dfrac{L}{\theta} \\ {a_y}^* \approx {a_n}^* = \dfrac{v_x^2}{R}, \end{cases} \tag{2}$$

where ω_w, r_w, v_x, L, θ, and R are wheel angular velocity, wheel radius, vehicle longitudinal velocity, wheelbase,

steering angle, and cornering radius, respectively. a_n^* is the target centripetal acceleration of the driver. It is approximately as same as the target lateral acceleration, a_y^*.

When the vehicle tends to be out of control such as drifting, the calculated target centripetal acceleration is much larger than the real one. Then this difference will be detected and limited by the two-dimensional envelope of the acceleration. Therefore the lateral traction force will be recovered to stabilize the vehicle.

3.3 Envelope control of motor torque

The vehicle acceleration a_v is

$$a_v = \sqrt{a_x^2 + a_y^2}. \tag{3}$$

a_x and a_y, the longitudinal and lateral vehicle accelerations, can be directly measured by an on-board accelerometer, which is widely used in today's road vehicles. Since a_v is a measured real one, it must be within the envelope of the achievable vehicle acceleration. Then the maximum available tangential (≈longitudinal) acceleration is:

$$a_t^* = \sqrt{a_v^2 - {a_n^*}^2}, \text{ if } |a_v| > |a_n^*|. \tag{4}$$

If $|a_v| < |a_n^*|$, the required normal (≈lateral) acceleration is out of the envelope. In this extreme case, a_t^*, the required tangential (≈longitudinal) acceleration should be simply zero for safety purposes.

Then the permissible maximum longitudinal traction torque T_f^* applied on the tire is:

$$T_f^* = Ma_t^* r_w, \tag{5}$$

where M is the vehicle mass. Here assume the drive motor torque T_m is K times of T_f^*, i.e.,

$$T_m = KT_f^*. \tag{6}$$

Real longitudinal traction torque T_f will eventually converge to T_f^* because under the envelope control the vehicle motion is stable. Then in the steady state v_w, v_x, and s can be calculated as:

$$\begin{cases} v_w = r_w \int \dfrac{(T_m - T_f^*)}{J_w} dt \\ v_x = \int \dfrac{T_f^*}{Mr_w} dt \\ s = 1 - \dfrac{v_x}{v_w} \end{cases}. \tag{7}$$

s can be represented as

$$s = 1 - \frac{\int \frac{T_f^*}{Mr_w} dt}{\int \frac{(T_m - T_f^*) r_w}{J_w} dt}. \tag{8}$$

Since $T_m = KT_f^*$, (8) can be further simplified as:

$$s = 1 - \frac{J_w}{(K-1)Mr_w^2}. \tag{9}$$

Therefore, as long as the vehicle parameters such as mass, M, wheel radius, r_w, and wheel inertia, J_w, are predefined, no matter how the road condition changes, the slip ratio keeps constant and is determined by the single parameter, K. For example, K can be determined to enable $s < 0.1$. Again under a target maximum permissible slip ratio s, the envelope of the drive motor torque command, T_m^*, is as equal as KT_f^*, namely

$$Max\{T_m^*\} = KT_f^*. \tag{10}$$

The overall control blockgiagram is shown in Fig. 6. The present permissible maximum traction torque T_f^* is first calculated based on the feedback signals of wheel angular velocity ω_w, steering angle θ, the longitudinal acceleration a_x, and the lateral acceleration a_y. Then the K times of T_f^* is the envelope or maximum permissible torque generated by the electric drive motor. If the motor torque command T_m^* from the driver is within this envelope, the torque envelope control will not interfere the control of the vehicle; while the T_m^* is out of the envelope, it will be effectively restricted because the original target motion of vehicle from the driver is beyond the traction capability.

Note that the electric motor torque envelope, KT_f^*, is distributed to the four wheels considering the weight transfer in the vehicle, as shown in (11)–(14). In the equations, l_r and l_f are the distances from rear axle and front axle to the Center of Gravity (COG), respectively; l is the wheelbase; l_w is the axle track; h_g is the height of COG, and F_{xG} and F_{yG} are the traction forces in longitudinal and lateral directions, respectively. The torque envelope is distributed to the wheels following the same ratios among the vertical forces or loads, F_{zFL}, F_{zFR}, F_{zRL}, and F_{zRR} ("z" is z axis; "F" is front; "R" is rear; "L" is left; "R" is right).

$$F_{zFL} = \frac{Mgl_r}{2l} - \frac{F_{xG}h_g}{2l} - \frac{F_{yG}h_g}{2l_w}, \tag{11}$$

$$F_{zFR} = \frac{Mgl_r}{2l} - \frac{F_{xG}h_g}{2l} + \frac{F_{yG}h_g}{2l_w}, \tag{12}$$

$$F_{zRL} = \frac{Mgl_f}{2l} + \frac{F_{xG}h_g}{2l} - \frac{F_{yG}h_g}{2l_w}, \tag{13}$$

$$F_{zRR} = \frac{Mgl_f}{2l} + \frac{F_{xG}h_g}{2l} + \frac{F_{yG}h_g}{2l_w}. \tag{14}$$

4. SIMULATION RESULTS

In this section, the proposed envelope control is verified by simulation under various representative driving conditions. The four-wheel-drive vehicle model was built on Matlab/Simulink that includes the longitudinal and lateral dynamics.

4.1 Driving in a straight line

For the driving in a straight line, the road surfaces are switched from the high friction surface (asphalt) to low friction surface (snowy), and then back to the high friction surface again:

(1) 0–10 s: asphalt road surface;
(2) 10–25 s: snowy road surface;
(3) 25–30 s: asphalt road surface.

Other conditions are:

(1) Initial velocity: 10 m/s;
(2) Original motor torque command: 200 Nm;
(3) Steering angle: 0 degree.

In the simulation the rear left tire is taken as an example, and the results are shown in Fig. 7 and Fig. 8. Without the envelope control, the large motor torque command T_m^* from the driver causes the slip ratio s to rapidly increase over the snowy surface and thus makes the motion of

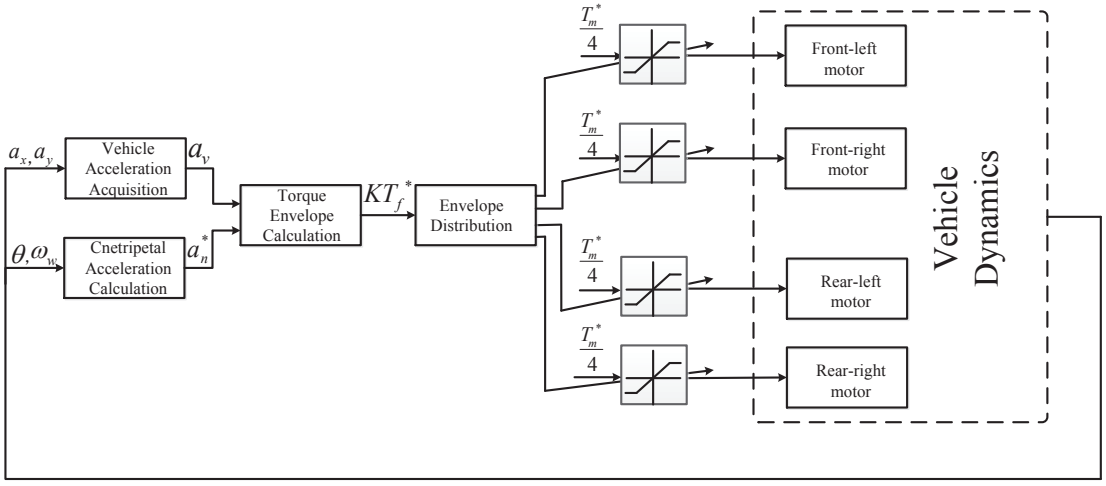

Fig. 6. Control blockdiagram

vehicle unstable. While with the envelope control, the drive motor torque is effectively suppressed at about 120 Nm over the snowy surface, and s also stays within its safe range.

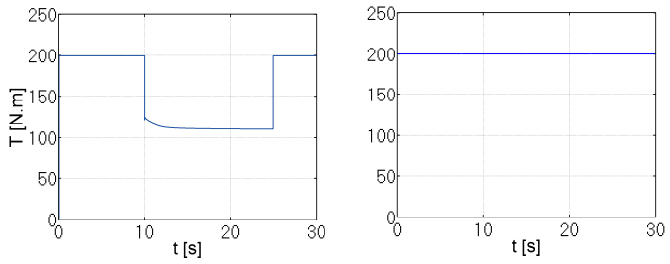

(a) With envelope control (b) Without envelope control.

Fig. 7. Final drive motor torque command when driving in a straight line.

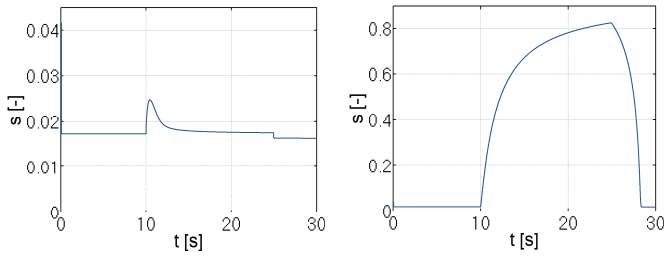

(a) With envelope control (b) Without envelope control

Fig. 8. Slip ratio.

4.2 Cornering

Two types of road surfaces are simulated during the vehicle cornering.

On asphalt road surface: Conditions in the simulation are:

(1) Road condition: asphalt;
(2) Initial velocity: 10 m/s;
(3) Original torque command: 150 Nm;
(4) Steering angle: 11.5 degree.

The simulation results are shown in Figs. 9–11, where the blue vehicle is with the envelope control and the red one is without control. Since the input steering angle is constant, the ideal vehicle trajectory should be a circle. The results show clearly that the trajectory of the blue vehicle is indeed a circle; while the trajectory of the red one is not. In addition, in Fig. 11 the solid and dotted circles represent the envelope of the traction force derived in this paper and the classical envelope (i.e., the tire friction ellipse), respectively. It can be seen that the derived envelope is always within the classical envelope and the centripetal acceleration (the small black arrow in the figure) of the blue vehicle becomes in normal direction. This shows the motion of the blue vehicle is stabilized.

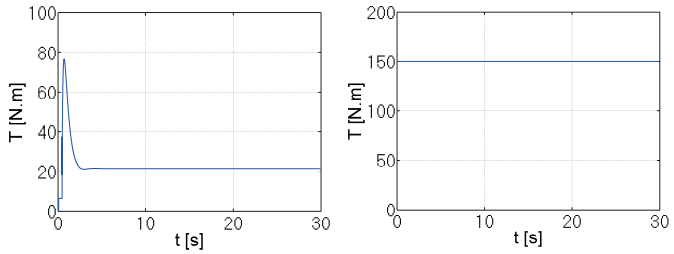

(a) With control (b) Without control

Fig. 9. Final drive motor torque command when cornering on asphalt road surface.

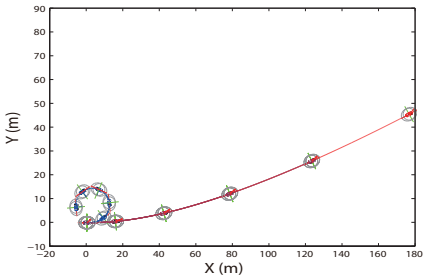

Fig. 10. Vehicle trajectory on the asphalt road surface (0–18 s)

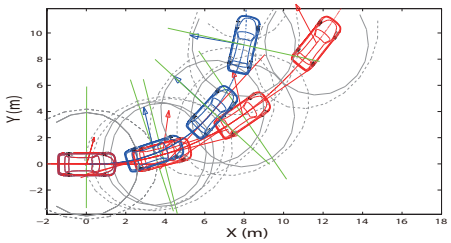

Fig. 11. Vehicle trajectory on the asphalt road surface (0–5 s)

On snowy road surface: Conditions in the simulation are:

(1) Road condition: snow;
(2) Initial velocity: 10 m/s;
(3) Original torque command: 60 Nm;
(4) Steering angle: 11.5 degree.

The simulation results are shown in Figs. 12–14. As shown in the figures, with the envelope control the final drive motor torque is effectively restricted in the low friction surface, and the trajectory of the vehicle is as same as the target circle. These results validate the effectiveness of the proposed envelope control when driving in a dangerous slippery road condition.

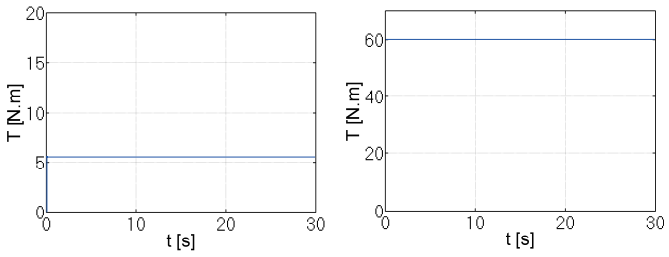

(a) With envelope control (b) Without envelope control

Fig. 12. Final drive motor torque command when cornering on snowy road surface.

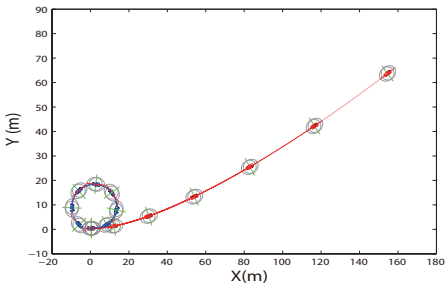

Fig. 13. Vehicle trajectory on the snowy road surface (0–16 s).

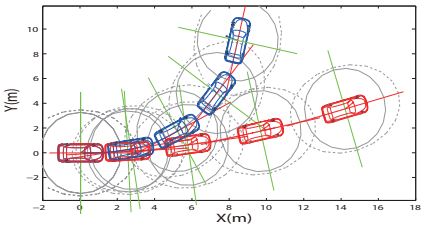

Fig. 14. Vehicle trajectory on the snowy road surface (0–5 s).

5. CONCLUSION

This paper discusses a new torque envelop control specified for electric vehicles. The control can effectively restrict the drive motor torque, and thus maintain the vehicle stability in extreme driving conditions. In addition, the proposed envelope control only needs feedback signals from a standard on-board accelerometer and encoders of the electric drive motors. Finally, the effectiveness of the proposed control is validated by simulation results under various driving conditions. The authors are now working on implementing the envelope control in an experimental four-wheel-drive electric vehicle. The experimental results and improvements will be reported later.

REFERENCES

Chen, Y. and Wang, J. (2013). Robust sideslip angle estimation for over-actuated electric vehicles: A linear parameter varying system approach. In *ASME 2013 Dynamic Systems and Control Conference*. American Society of Mechanical Engineers, Palo Alto, California, USA.

Hori, Y., Toyoda, Y., and Tsuruoka, Y. (1998). Traction control of electric vehicle: Basic experimental results using the test EV UOT electric marchII. *IEEE Trans. Ind. Applicat.*, 34(5), 1131–1138.

Liebemann, E., Meder, K., Schuh, J., and Nenninger, G. (2004). Safety and performance enhancement: The Bosch electronic stability control (ESP). *SAE Paper*, 20004, 21–0060.

Nam, K., Fujimoto, H., and Hori, Y. (2012). Lateral stability control of in-wheel-motor-driven electric vehicles based on sideslip angle estimation using lateral tire force sensors. *IEEE Trans. Veh. Technol.*, 61(5), 1972–1985.

Pacejka, H.B. and Bakker, E. (1992). The magic formula tyre model. *Vehicle system dynamics*, 21(S1), 1–18.

Siegwart, R., Nourbakhsh, I.R., and Scaramuzza, D. (2011). *Introduction to autonomous mobile robots*. MIT press.

Tahami, F., Kazemi, R., and Farhanghi, S. (2003). A novel driver assist stability system for all-wheel-drive electric vehicles. *IEEE Trans. Veh. Technol.*, 52(3), 683–692.

Van Zanten, A.T. (2000). Bosch ESP systems: 5 years of experience. Technical report, SAE Technical Paper.

Wu, X., Ma, C., Xu, M., Zhao, Q., and Cai, Z. (2015). Single-parameter skidding detection and control specified for electric vehicles. *Journal of the Franklin Institute*, 352(2), 724–743.